



CHORUS

This is the accepted manuscript made available via CHORUS. The article has been published as:

Calculation of antihydrogen formation via antiproton scattering with excited positronium

C. M. Rawlins, A. S. Kadyrov, A. T. Stelbovics, I. Bray, and M. Charlton

Phys. Rev. A **93**, 012709 — Published 19 January 2016

DOI: [10.1103/PhysRevA.93.012709](https://doi.org/10.1103/PhysRevA.93.012709)

Calculation of antihydrogen formation via antiproton scattering with excited positronium

C. M. Rawlins, A. S. Kadyrov, A. T. Stelbovics, I. Bray

*Curtin Institute for Computation and Department of Physics, Astronomy and Medical Radiation Sciences,
Curtin University, GPO Box U1987, Perth, WA 6845, Australia*

M. Charlton

Department of Physics, College of Science, Swansea University, SA2 8PP, United Kingdom

The two-centre convergent close-coupling method is used to calculate antihydrogen ($\bar{\text{H}}$) formation via positronium (Ps) scattering on antiprotons (\bar{p}) at near threshold energies. For excited Ps of energy ε , the $1/\varepsilon$ behavior of the $\bar{\text{H}}$ formation cross sections is valid strictly only at the respective threshold, as is the $1/\sqrt{\varepsilon}$ behaviour for Ps in the ground state. Simple equations are given for the $\bar{\text{H}}(n \leq 4)$ formation cross sections from Ps($n \leq 3$) from zero to around 0.1 eV above threshold. Some of the implications of using \bar{p} -Ps collisions to form antihydrogen in beams, and held in traps, are discussed.

PACS numbers:

I. INTRODUCTION

The study of antimatter has been of great interest for several decades, and typically involves comparisons of the properties of particles and antiparticles as tests of symmetry (see e.g., [1]). More recently antihydrogen, the positron-antiproton bound state, has become available for study (see [2] for a topical review). While some matter/antimatter properties are well known, such as certain charge-to-mass ratios [1], the quest to understand the apparent asymmetry implied by the predominance of matter over antimatter in the Universe has motivated continued study. In particular, spectroscopic investigations of $\bar{\text{H}}$ promise to provide sensitive tests of the CPT symmetry [2–5], and there are also current efforts to probe the gravitational properties of antimatter, including $\bar{\text{H}}$ [6–11]. Within the framework of General Relativity, the weak equivalence principle states that if a particle is only submitted to gravity then the trajectory of that particle is independent of its charge and internal structure [6]. Thus, it is assumed that the gravitational behaviour of matter and antimatter are equivalent, but this has never been directly tested by experiment. Since the strength of gravitational interaction is much lower than that of electromagnetism the weak equivalence principle for antimatter can only be accurately tested using neutral species, with the simplest case being $\bar{\text{H}}$. It is thus timely to consider mechanisms by which $\bar{\text{H}}$ may be produced in the laboratory in a manner conducive to investigations of its properties.

One such mechanism arises from the interaction between antiprotons and positronium (Ps, the e^+e^- bound state) atoms. A possible result of their interaction is the production of $\bar{\text{H}}$ by the reaction [3, 12, 13]



From the point of view of theory this is entirely equivalent to $p + \text{Ps} \rightarrow \text{H} + e^+$, and so cross sections are obtainable from positron-hydrogen scattering.

The AEGIS $\bar{\text{H}}$ group at CERN have plans to produce the anti-atom in Rydberg states by this method [9, 10, 14]. This is largely because it is generally believed that the cross section for this process scales by n_{Ps}^4 where n_{Ps} is the principal quantum number of the Ps [13, 15], implying that the use of Ps in a Rydberg state in reaction 1 would efficiently produce antihydrogen in a Rydberg state. Use of reaction 1 was also proposed by Walz and Hänisch [16] with the resultant $\bar{\text{H}}$ to undergo further collisions with the Ps target to produce the antimatter equivalent of the hydride ion, namely $\bar{\text{H}}^+$. The ions are then held in an ion trap where they are sympathetically cooled (using co-trapped laser cooled ions), before the positron is removed by photoionisation, thereby allowing the remaining $\bar{\text{H}}$ to fall freely in the Earth's gravitational field. This is the aim of the GBAR group [7, 8, 17].

Both the AEGIS and GBAR experiments pose significant technical challenges. Thus, it is useful to have accurate scattering cross sections available for reaction 1 over as wide an energy range, and for as many initial Ps and final $\bar{\text{H}}$ states, as possible. The exothermic nature of the reaction implies that the $\bar{\text{H}}$ formation cross sections for this mechanism increase as the energy of the Ps atom is lowered. Therefore, if near-zero energy Ps could be used for scattering on cold, trapped antiprotons then the yield of cold $\bar{\text{H}}$ would be enhanced. According to Wigner [18] the cross sections for such a process behave as $1/\sqrt{\varepsilon}$ as $\varepsilon \rightarrow 0$ where ε is the energy of the Ps projectile, and this is observed for the case of Ps(1s). However, for excited Ps states, owing to the degeneracy of their energy levels, the low energy behavior is modified to $1/\varepsilon$ [19, 20]. This behavior was confirmed in our recent work [21]. Furthermore, it was found that the concomitant dramatic rise in the cross sections for reaction 1 occurred within an exper-

imentally viable range, thus motivating a more detailed presentation of our data (see section III).

A theory for determining the cross sections for energies where the $1/\varepsilon$ relationship is valid must be developed to produce reliable guideline data for experiment. An ideal starting point would be the scattering of positrons on hydrogen atoms, since Ps formation by this method is, as mentioned above, simply the reverse of hydrogen formation by scattering positronium on protons [22]. Various theoretical methods have been used to determine the cross sections for (anti)hydrogen formation by the reaction (1). Benchmark results at low energies involving only ground states were obtained using a variational approach by Humberston *et al.* [23], and reported in full by Kadyrov *et al.* [21]. Several other approaches involve expanding the total wave function in terms of H and Ps states. There are time-independent close-coupling (CC) approaches [24–28], time-dependent close-coupling (TDCC) [29] and the Continuum Distorted Wave - Final State (CDW-FS) method [30] to name a few. Mitroy [24] implemented both centres into a close-coupling method for positron scattering on hydrogen and later positronium scattering on protons [27]. Work was also done on formation of antihydrogen [25, 28] using a Unitarised Born Approximation (UBA). The TDCC solves the scattering wave function with a wave packet time dependently. The CDW-FS method describes the states using Coulomb wave functions with exact boundary conditions. Nevertheless, the challenge of yielding accurate results for various initial states at low energies of interest in experiment remains to be met.

The two-centre convergent close-coupling (CCC) method of Kadyrov and Bray [31] expands the total wave function in terms of Laguerre-based atomic and Ps states of negative and positive energies $\epsilon_n^{(H)}$ and $\epsilon_n^{(Ps)}$, respectively (where here n denotes, as appropriate, the Ps or H principal quantum number). The key idea is to obtain convergence with systematic increase of the size of the bases N_l^{Ps} and N_l^H for $l \leq l_{\max}$. One of the remarkable aspects of the formulation is the capacity to check for internal validation by ensuring consistency between one- and two-center results for every partial wave of the total orbital angular momentum [32]. Briefly, if we define the “extended Ore gap” to be between the Ps formation and the ionization thresholds, then for incident positron energies E_0 outside this gap the two approaches should yield the same results. This is because the one-center calculation is formally valid outside the extended Ore gap, with the positive-energy atomic states corresponding to both the (inseparable in this approach) Ps formation and break-up collision processes. Specifically, denoting the corresponding calculated cross sections as $\sigma_{fi}^{(1)}$ and $\sigma_{fi}^{(2)}$, for $E_0 < 6.8$ eV

$$\sigma_{ii}^{(1)} = \sigma_{ii}^{(2)}, \quad (2)$$

and for $E_0 > 13.6$ eV

$$\begin{aligned} \sigma_{fi}^{(1)} &= \sigma_{fi}^{(2)}, \text{ where } \epsilon_f^{(H)} < 0, \text{ and} & (3) \\ \sum_{\epsilon_f^{(H)} > 0} \sigma_{fi}^{(1)} &= \sum_{\epsilon_f^{(H)} > 0} \sigma_{fi}^{(2)} + \sum_{\epsilon_f^{(Ps)} < 0} \sigma_{fi}^{(2)} + \sum_{\epsilon_f^{(Ps)} > 0} \sigma_{fi}^{(2)}. \end{aligned}$$

The latter is the statement that electron-loss (ionization) cross sections in the one-state calculation should be the same as those obtained in the two-center calculations, which are composed of the three specified components. The first ($\epsilon_f^{(H)} > 0$) and the third ($\epsilon_f^{(Ps)} > 0$) components correspond to the break-up processes in two-center calculations. Nevertheless, due to the unitarity of the close-coupling formalism there is no double counting. However, as bases sizes increase, the two-center equations become particularly ill-conditioned.

Checking the elastic, excitation and electron-loss cross sections for each partial wave at energies outside the extended Ore gap is a very valuable validation of both implementations. It tells us when the one-center approach may be used to yield accurate results such as given in [33–37], where the effect of Ps formation (virtual or real) manifests itself with slow convergence with increasing l_{\max} . However, either within the extended Ore gap, or whenever explicit Ps-formation results are required, only the two-center calculations are capable of yielding the required cross sections.

Here we are interested in the rearrangement collision process, and so only two-center CCC calculations are applicable. From the self-consistency checks [32] we know that they should be valid at all energies. Such calculations produce accurate results down to 10^{-5} eV above the Ps(1s) threshold for H(1s) formation using a relatively small basis [38], and also for excited states requiring larger bases [21]. For brevity of presentation, the latter gave results for the summed (anti)hydrogen formation. We now take the opportunity to present the full state-to-state cross sections, and provide simple fitting formulae for ease of use at low energies.

II. THEORY

Details for positron scattering on atoms using the two-center CCC method are given by Kadyrov and Bray [31]. Briefly, to represent the atomic and Ps states independently the complete Laguerre basis

$$\begin{aligned} \xi_{kl}(r) &= \left(\frac{\lambda_l (k-1)!}{(2l+1+k)!} \right)^{1/2} & (4) \\ &\times (\lambda_l r)^{l+1} \exp(-\lambda_l r/2) L_{k-1}^{2l+2}(\lambda_l r) \end{aligned}$$

is utilised, where $L_{k-1}^{2l+2}(\lambda_l r)$ are the associated Laguerre polynomials, $l \leq l_{\max}$ is the orbital angular momentum of the target (H or Ps) state, λ_l is the exponential factor and k ranges from 1 to the basis size N_l . A linear combination of the basis functions is then used to diagonalize

the target Hamiltonian H_T

$$\langle \phi_f^{(T)} | H_T | \phi_i^{(T)} \rangle = \epsilon_f^{(T)} \langle \phi_f^{(T)} | \phi_i^{(T)} \rangle = \epsilon_f^{(T)} \delta_{fi}. \quad (5)$$

This is done for both H and Ps targets to obtain the pseudostates used to expand the total wave function of the scattering system. With increasing N_l the negative-energy states converge to the true discrete eigenstates, while the positive-energy states provide an increasingly dense discretization of the continuum.

Using these pseudostates, a set of momentum-space coupled Lippmann-Schwinger equations are solved to determine the transition matrix elements

$$T_{\gamma',\gamma}(\mathbf{q}_{\gamma'}, \mathbf{q}_{\gamma}) = V_{\gamma',\gamma}(\mathbf{q}_{\gamma'}, \mathbf{q}_{\gamma}) + \sum_{\gamma''}^{N_H + N_{Ps}} \int \frac{d\mathbf{q}_{\gamma''}}{(2\pi)^3} \times \frac{V_{\gamma',\gamma''}(\mathbf{q}_{\gamma'}, \mathbf{q}_{\gamma''}) T_{\gamma'',\gamma}(\mathbf{q}_{\gamma'', \mathbf{q}_{\gamma}})}{E + i0 - \epsilon_{\gamma''} - q_{\gamma''}^2 / (2M_{\gamma''})}, \quad (6)$$

where E is the total energy, \mathbf{q}_{γ} is the momentum of the free particle γ with respect to the centre of mass of the bound pair in channel γ (H or Ps), ϵ_{γ} is the energy of the bound pair, M_{γ} is its reduced mass and $V_{\gamma',\gamma}$ is the effective potential. The coupled equations are solved using the partial-wave expansion in total orbital angular momentum.

The convergence of the results is checked against increasing N_l and l_{\max} for both H and Ps. With explicit Ps included large l_{\max} are not required, as they are in one-center calculations. Here we have taken $l_{\max}^{(H)} = 3$ and $l_{\max}^{(Ps)} = 2$ (see below). Since the Ps and H expansions are non-orthogonal, with a clear overlap for the breakup process, the problem becomes highly ill-conditioned as the number of states increases. Hence, arbitrarily high bases cannot be taken. To systematically check the convergence we fixed $\lambda_l^{(H)} = 1$ and $\lambda_l^{(Ps)} = 0.5$, and set $N_l = N_0 - l$ with $N_l^{(H)} = N_l^{(Ps)}$, leaving only one parameter (N_0) to vary. Calculations were performed with $N_0 = 10, 11, 12$, with the energies for the latter case presented in Fig. 1.

For $N_l = 12 - l$, with above-mentioned λ , the H and Ps states are accurate for $n \leq 5$. Our initial states are denoted as $Ps(nl)$. For $Ps(1s)$ as the initial state we require a positron energy in excess of 6.8 eV, leading to the Ps energy $\epsilon > 0$. At threshold, formation of only the lower energy $H(1s)$ state is possible. At the threshold of the $Ps(n=2)$ states only formation of $H(n \leq 2)$ states are possible, whilst for $Ps(n=3)$ states formation of $H(n \leq 4)$ are energetically allowed. The additional H n -level arises (see figure 1) due to the interplay of the H and Ps eigenenergies, which vary, as is well-known, according to n^{-2} and $n^{-2}/2$, respectively. For this reason we chose $l_{\max}^{(H)} = 3$ and $l_{\max}^{(Ps)} = 2$ so that we could achieve accurate $Ps(n \leq 3)$ to $H(n \leq 4)$ cross sections whilst keeping the size of the calculations manageable to minimize ill-conditioning.

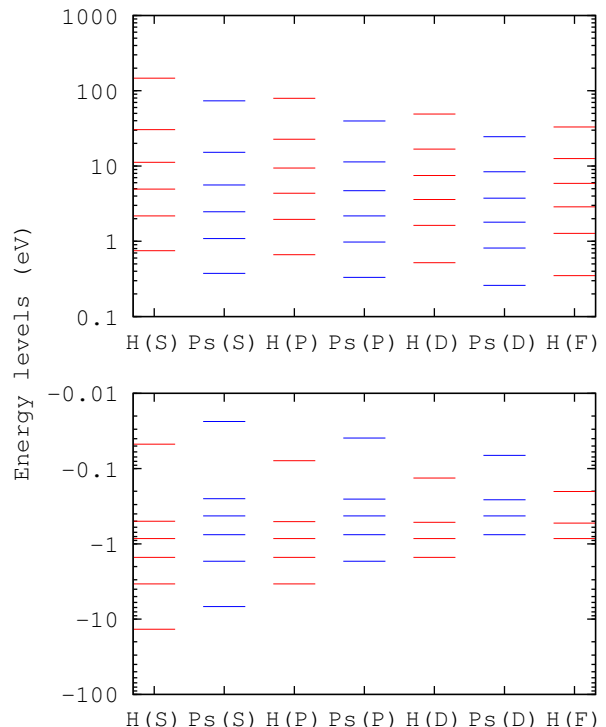


FIG. 1: (Color online) Energy levels of the positronium and hydrogen states used in the two-center CCC calculations. They were obtained by solving Eq. (5) for both H and Ps with $N_l = 12 - l$, see text.

III. RESULTS

The data for (anti)hydrogen formation in the scattering of $Ps(1s)$ on (anti)protons are presented in figure 2 where, as is evident from figure 1, the only hydrogen state available near zero energy is $H(1s)$. The remaining states do not open up until around 5 eV of Ps kinetic energy. The excellent agreement with the variational calculations of Humberston *et al.* [23] (which are not shown in figure 1) has already been discussed by Kadyrov *et al.* [21]. Here we concentrate on establishing a simple formula to fit the low-energy data. As discussed in section I, the cross sections for $H(1s)$ near threshold behave as $1/\sqrt{\epsilon}$, in accordance with Wigner [18]. This is represented by the solid line over the data points, obtained from a least squares fit to the function $\sigma_{H(nl)} = \epsilon^{-1/2}(a + b\epsilon^{1/2} + c\epsilon)$ from zero to 0.01 eV, with the values of a , b and c given in table I. The fact that b is comparable to a indicates that the threshold law is valid strictly only at threshold. Nevertheless, the simple formula can be used across the three orders of magnitude of the presented low energies.

Whereas $H(1s)$ formation from $Ps(1s)$ is an exothermic reaction, and so the cross section tends to infinity at threshold, the formation of $H(n > 1)$ requires a loss of Ps kinetic energy. Consequently, their respective thresholds are non-zero and the cross sections typically rise rapidly from zero to a maximum, and then slowly

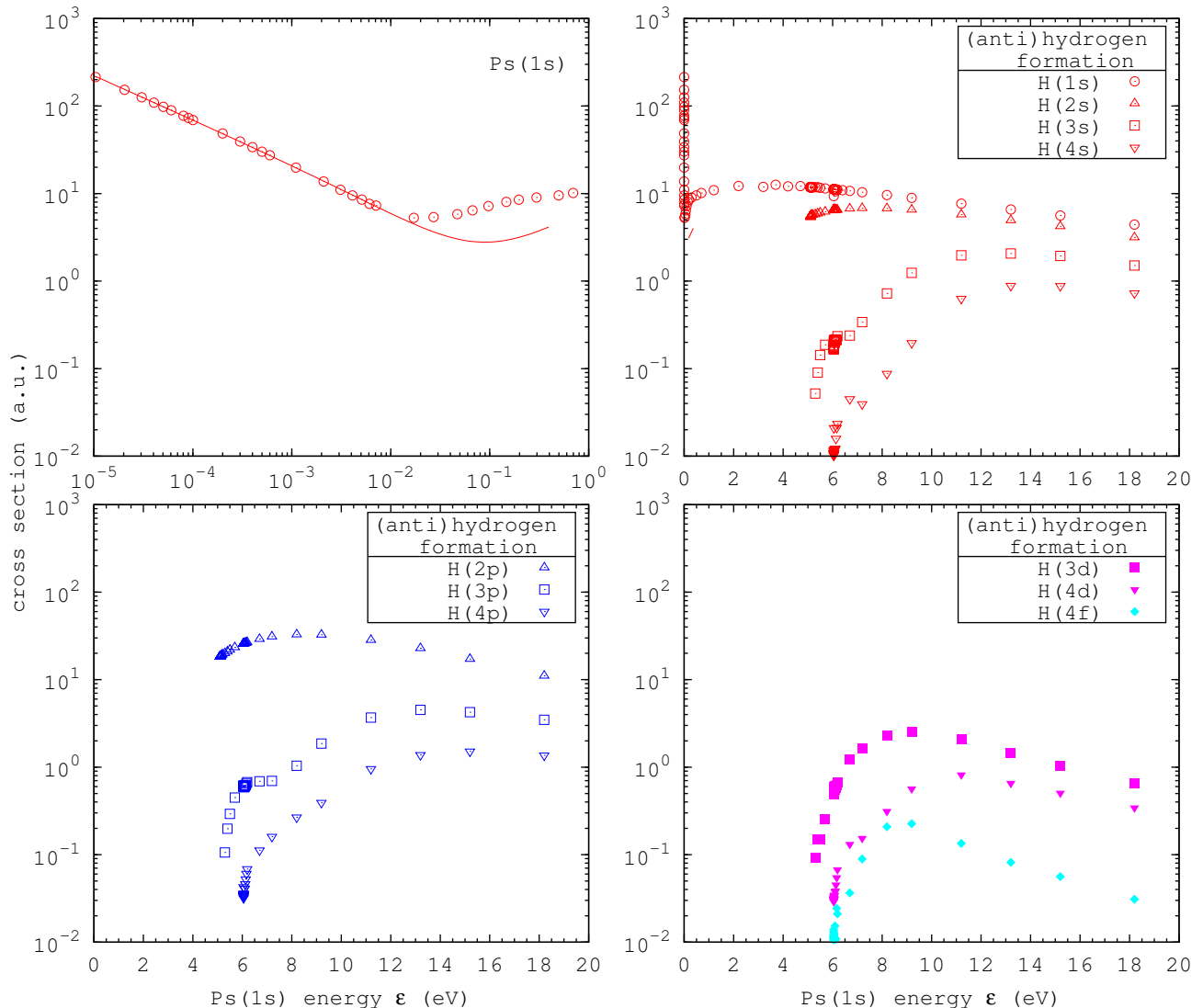


FIG. 2: (Color online) The cross sections for positronium in the $1s$ state scattering on (anti)protons to form (anti)hydrogen. The data presented are for transitions open near zero energies (top left), and then transitions across the full energy range of the calculation into s -states (top right), p -states (bottom left) and d - and f -states (bottom right). The solid line for the near zero energy results is a least squares fit of the data up to 0.01eV (see text) with the fitting parameters given in table I.

fall again. Whereas we expect the actual cross sections to vary smoothly as a function of energy we occasionally find outlying points. This is a manifestation of the ill-conditioned nature of the problem. Data obtained using smaller values of N_0 contain fewer examples of this behavior, but show somewhat greater pseudoresonance structure. The present results are generally at the $\pm 5\%$ level of convergence.

The data for $\text{Ps}(2s)$ initial state are presented in Fig. 3. For $\text{Ps}(n=2)$ the channels for formation of $\text{H}(n \leq 2)$ are open at zero energy. The $\text{H}(n=2)$ formation cross sections (top and bottom left) are massively increased compared to the $\text{Ps}(1s)$ case of figure 2. Formation of $\text{H}(1s)$ is two orders of magnitude less likely than $\text{H}(2s)$ and $\text{H}(2p)$, which are broadly similar. These enhancements can be attributed to a number of sources: (i) the increased size and polarizability of the Ps and H states, (ii) the lower

energy difference between $\text{Ps}(n=2)$ and $\text{H}(n=2)$ levels and (iii) the emergence of the $1/\varepsilon$ threshold behavior. The $\text{Ps}(1s)$ data exhibited the $1/\sqrt{\varepsilon}$ behavior at low energies, however this is altered by the introduction of the degenerate $\text{H}(n=2)$ states to $1/\varepsilon$ in agreement with Fabrikant [19]. Accordingly, the solid lines in Fig. 3 are a least squares fit of the function $\sigma_{\text{H}(nl)} = \varepsilon^{-1}(a + b\varepsilon + c\varepsilon^2)$ to the data from zero to 0.1eV , with the fitted coefficients given in table II. The quantitative similarity is immediately evident for the $\text{H}(2s)$ and $\text{H}(2p)$ cross sections. Once more, the magnitude of the b coefficients indicates that the laws are only strictly valid at threshold.

The (anti)hydrogen formation cross sections for the $\text{Ps}(2p)$ initial state are given in Fig. 4, with the corresponding least square fits given in Table III. There are only quantitative differences with the results for the $\text{Ps}(2s)$ case. The low-energy cross sections are somewhat

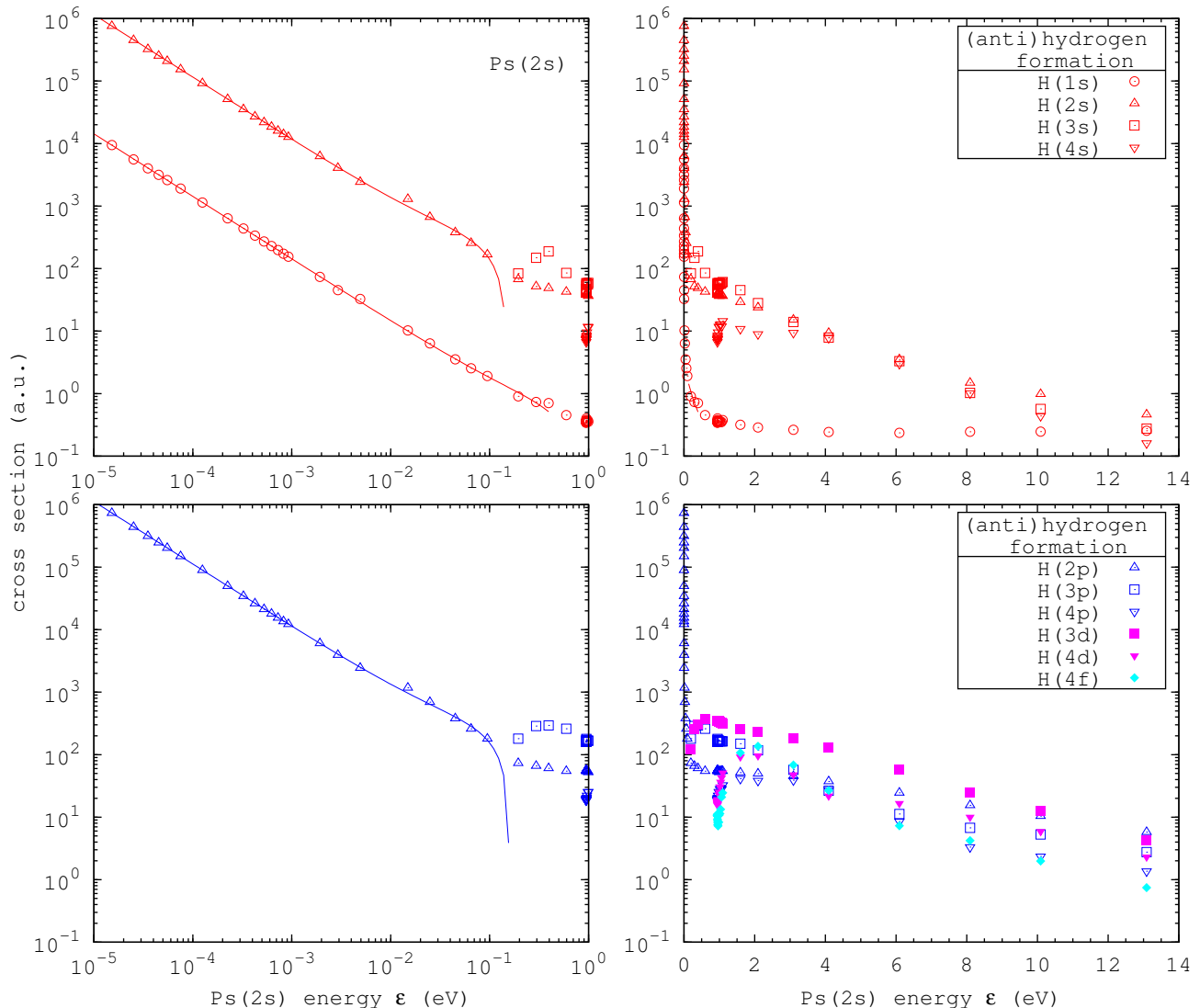


FIG. 3: (Color online) The cross sections for positronium in the 2s state scattering on (anti)protons to form (anti)hydrogen. The left side data are for scattering near zero energies for formation of hydrogen in an s (top) or p state (bottom). The right side data are across a larger energy range for formation in s (top) or p , d or f states (bottom). The solid lines for the near zero energy results are least squares fits of the data up to 0.1eV with the fitted parameters given in table II.

TABLE I: Cross sections $\sigma_{H(nl)} = \varepsilon^{-1/2}(a + b\varepsilon^{1/2} + c\varepsilon)$ (a.u.) for near zero energy ε (eV) Ps($1s$) incident on (anti)protons, as shown by the solid line in figure 2. These values were obtained by a least squares fit of the data up to 0.01eV. The numbers in brackets indicate the power of 10.

	a	b	c
$\sigma_{H(1s)}$	7.087[-1]	-1.958[+0]	7.926[+0]

smaller, as can be seen when comparing the a coefficients in tables II and III. Thus, the overall qualitative behavior of the data for the Ps($n = 2$) initial states appears to be quite similar, being dominated by the effects of the degenerate $n = 2$ energies.

The results for Ps($n = 3$) are considerably more detailed. In these cases all of the H($n \leq 4$) states are open

TABLE II: Cross sections $\sigma_{H(nl)} = \varepsilon^{-1}(a + b\varepsilon + c\varepsilon^2)$ (a.u.) for near zero energy ε (eV) Ps($2s$) incident on (anti)protons, as shown by the solid lines in figure 3. These values were obtained by a least squares fit of the data up to 0.1eV. The numbers in brackets indicate the power of 10.

	a	b	c
$\sigma_{H(1s)}$	1.429[-1]	4.528[-1]	-7.623[-1]
$\sigma_{H(2s)}$	1.154[+1]	2.452[+2]	-2.197[+3]
$\sigma_{H(2p)}$	1.120[+1]	2.417[+2]	-1.992[+3]

at zero incident energy. We begin with Ps($3s$) given in Fig. 5, with the formulae for the fitted data shown in table IV. We see that there is another order of magnitude increase in the largest cross sections, this time to the H($n = 4$) states. From Fig. 1, it is evident that the Ps($n = 3$) energies are only marginally higher than those

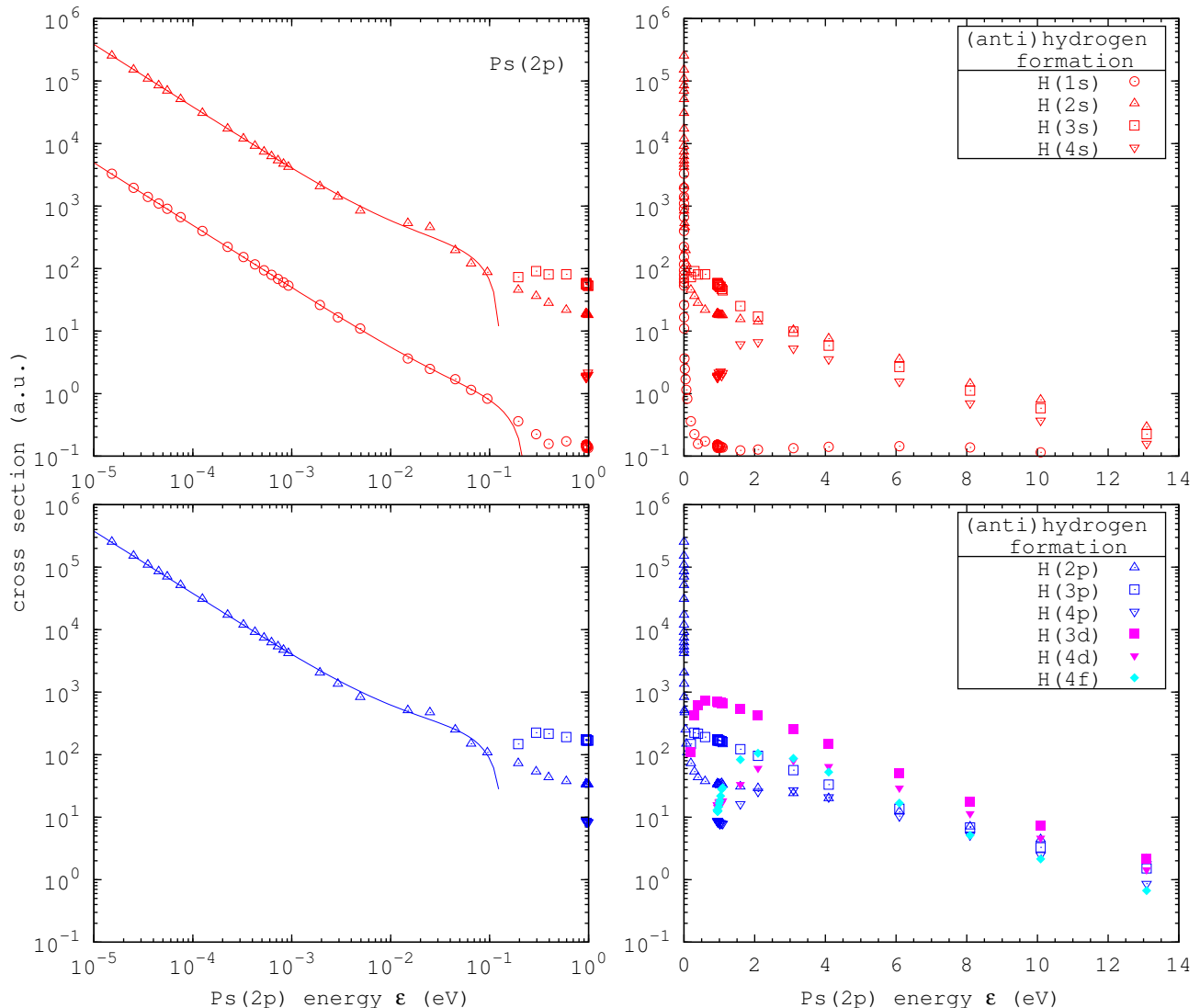


FIG. 4: (Color online) The cross sections for positronium in the $2p$ state scattering on (anti)protons to form (anti)hydrogen. The left side data are for scattering near zero energies for formation of hydrogen in an s (top) or p state (bottom). The right side data are across a larger energy range for formation in s (top) or p , d or f states (bottom). The solid lines for the near zero energy results are least squares fits of the data up to 0.1eV with the fitted parameters given in table III.

TABLE III: Cross sections $\sigma_{\text{H}(nl)} = \varepsilon^{-1}(a + b\varepsilon + c\varepsilon^2)$ (a.u.) for near zero energy ε (eV) $\text{Ps}(2p)$ incident on (anti)protons, as shown by the solid lines in figure 4. These values were obtained by a least squares fit of the data up to 0.1eV . The numbers in brackets indicate the power of 10.

	a	b	c
$\sigma_{\text{H}(1s)}$	4.927[-2]	6.586[-1]	-3.663[+0]
$\sigma_{\text{H}(2s)}$	3.849[+0]	2.215[+2]	-1.953[+3]
$\sigma_{\text{H}(2p)}$	3.772[+0]	2.672[+2]	-2.188[+3]

for $\text{H}(n=4)$. Such a small difference contributes to the enhanced cross sections, as well as the increased size and polarizability of the incident Ps . There are only minor quantitative differences between the cross sections for the formation of $\text{H}(n=4)$ states, with those for $\text{H}(4s)$ being somewhat smaller than the others. Interestingly, the

$\text{H}(4d)$ and $\text{H}(4f)$ cross sections are barely distinguishable at the low energies, as is also apparent from table IV. The threshold relationships hold strictly at threshold, and the given formulae are accurate up to 0.1eV . The $\text{H}(n=3)$ cross sections are an order of magnitude lower than those for $\text{H}(n=4)$, and those for lower values of n seem to drop by a further order of magnitude.

Figure 6 shows the $\text{H}(n \leq 4)$ formation cross sections for the $\text{Ps}(3p)$ initial state, with details of the fitted formulae given in table V. The qualitative behavior of the data is much the same as for the $\text{Ps}(3s)$ results. Quantitative differences may be readily extracted using the a coefficients in the corresponding tables.

Finally, the cross sections for $\text{H}(n \leq 4)$ formation for the case of the $\text{Ps}(3d)$ initial state are presented in Fig. 7, with the corresponding formulae from least-square fits given in table VI. We see no qualitative change from the

TABLE IV: Cross sections $\sigma_{\text{H}(nl)} = \varepsilon^{-1}(a + b\varepsilon + c\varepsilon^2)$ (a.u.) for near zero energy ε (eV) Ps($3s$) incident on (anti)protons, as shown by the solid lines in figure 5. These values were obtained by a least squares fit of the data up to 0.1eV. The numbers in brackets indicate the power of 10.

	a	b	c
$\sigma_{\text{H}(1s)}$	7.724[-3]	-4.788[-2]	7.442[-1]
$\sigma_{\text{H}(2s)}$	3.218[-1]	3.566[+0]	-2.728[+1]
$\sigma_{\text{H}(2p)}$	4.437[-1]	1.026[+0]	1.584[+1]
$\sigma_{\text{H}(3s)}$	5.220[+0]	4.519[+1]	-4.769[+2]
$\sigma_{\text{H}(3p)}$	8.626[+0]	1.066[+2]	-1.310[+3]
$\sigma_{\text{H}(3d)}$	3.664[+0]	4.252[+1]	-2.182[+2]
$\sigma_{\text{H}(4s)}$	3.892[+1]	-2.019[+2]	4.573[+3]
$\sigma_{\text{H}(4p)}$	1.178[+2]	-7.584[+2]	1.164[+4]
$\sigma_{\text{H}(4d)}$	1.097[+2]	1.235[+3]	-1.174[+4]
$\sigma_{\text{H}(4f)}$	8.713[+1]	1.650[+3]	1.167[+4]

TABLE V: Cross sections $\sigma_{\text{H}(nl)} = \varepsilon^{-1}(a + b\varepsilon + c\varepsilon^2)$ (a.u.) for near zero energy ε (eV) Ps($3p$) incident on (anti)protons, as shown by the solid lines in figure 6. These values were obtained by a least squares fit of the data up to 0.1eV. The numbers in brackets indicate the power of 10.

	a	b	c
$\sigma_{\text{H}(1s)}$	3.892[-3]	5.562[-3]	1.994[-1]
$\sigma_{\text{H}(2s)}$	2.829[-1]	2.184[+0]	-9.661[+0]
$\sigma_{\text{H}(2p)}$	4.027[-1]	2.522[+0]	1.377[+0]
$\sigma_{\text{H}(3s)}$	3.628[+0]	1.289[+1]	6.323[+1]
$\sigma_{\text{H}(3p)}$	7.433[+0]	5.333[+1]	-5.490[+1]
$\sigma_{\text{H}(3d)}$	4.759[+0]	2.311[+1]	1.052[+2]
$\sigma_{\text{H}(4s)}$	2.382[+1]	1.104[+2]	-3.021[+2]
$\sigma_{\text{H}(4p)}$	7.705[+1]	8.548[+1]	-3.670[+2]
$\sigma_{\text{H}(4d)}$	7.906[+1]	4.618[+2]	1.262[+2]
$\sigma_{\text{H}(4f)}$	8.257[+1]	2.160[+3]	3.257[+3]

other $n = 3$ cases, though quantitatively the cross sections are somewhat lower in magnitude.

This completes our presentation of H($n \leq 4$) formation cross sections from Ps($n \leq 3$) initial states incident on (anti)protons at the lower energies of interest

TABLE VI: Cross sections $\sigma_{\text{H}(nl)} = \varepsilon^{-1}(a + b\varepsilon + c\varepsilon^2)$ (a.u.) for near zero energy ε (eV) Ps($3d$) incident on (anti)protons, as shown by the solid lines in figure 7. These values were obtained by a least squares fit of the data up to 0.1eV. The numbers in brackets indicate the power of 10.

	a	b	c
$\sigma_{\text{H}(1s)}$	1.048[-3]	5.107[-3]	7.025[-2]
$\sigma_{\text{H}(2s)}$	1.214[-1]	2.821[-1]	8.805[+0]
$\sigma_{\text{H}(2p)}$	1.813[-1]	1.274[+0]	4.103[+0]
$\sigma_{\text{H}(3s)}$	1.213[+0]	2.412[+0]	2.570[+2]
$\sigma_{\text{H}(3p)}$	2.733[+0]	1.364[+1]	5.353[+2]
$\sigma_{\text{H}(3d)}$	2.343[+0]	3.535[+1]	-2.597[+1]
$\sigma_{\text{H}(4s)}$	8.463[+0]	7.395[+1]	-5.959[+2]
$\sigma_{\text{H}(4p)}$	2.722[+1]	1.443[+2]	-4.255[+2]
$\sigma_{\text{H}(4d)}$	2.662[+1]	2.549[+2]	3.892[+3]
$\sigma_{\text{H}(4f)}$	3.996[+1]	2.852[+3]	-6.547[+3]

to experiment. It is clear from the trends exhibited in our data that transitions between Ps and H states with near-matching energies for as high values of n as possible will yield the largest cross sections. However, the energy interplay makes extrapolation procedures problematic. Clearly there is incentive to increase the size of the calculations. It would be particularly interesting to allow for Ps($n = 5$) with H($n = 7$). In this case the energy difference is very small (0.0056 eV), and so should yield particularly large cross sections. To achieve this we have to run with $N_0 \approx 20$. This is not practical with the present implementation of the CCC code, however there are currently two developments that should assist in addressing this issue. First, following the successful analytical treatment of the singularities in the CCC equations in a model problem [39], we expect to reduce ill-conditioning when implemented for the full (present) problem. The requirement to yield results close to thresholds requires treatment of principal-value singularities very close to zero. Eliminating them would be advantageous. Secondly, implementation of arbitrary precision numerical approaches [40], as has been done for proton-hydrogen scattering [41], will also assist in that regard.

IV. DISCUSSION

In this section we present analyses in which our calculated cross sections are used to estimate the yields of $\bar{\text{H}}$ atoms from reaction 1 in geometries which result, broadly speaking, in the production of (i) an $\bar{\text{H}}$ beam, and (ii) trapped $\bar{\text{H}}$. In both cases the most relevant starting Ps states are the $1s$, $2p$, $3p$, and $3d$ states. The $2p$ and $3p$ states can be reached efficiently from the ground state by single photon transitions at 243 nm (see e.g., [42, 43]) and 205 nm [44, 45] respectively, whilst the $3d$ level can be accessed via a transition involving two 410 nm photons.

A. Antihydrogen Beams

Atomic and molecular beams have had an important role in the development of physics (see e.g., [46, 47]). Nowadays they are used routinely for many purposes, including the population of optical and magneto-optical traps found in a wide variety of investigations in contemporary atomic/molecular physics. By contrast, in antihydrogen work to date there have been no physics studies using directed fluxes of the anti-atom, though progress towards this goal is ongoing (see below). Currently, $\bar{\text{H}}$ atoms are created in Penning trap-like environments in which strong (typically of the order of tesla in magnitude) magnetic fields are present to confine the constituent antiparticles. Given the well-known effects of such fields on the spectral properties of atomic species (see e.g., [48]) a major motivation to produce $\bar{\text{H}}$ beams is to facilitate measurements of its properties in a field-free region to

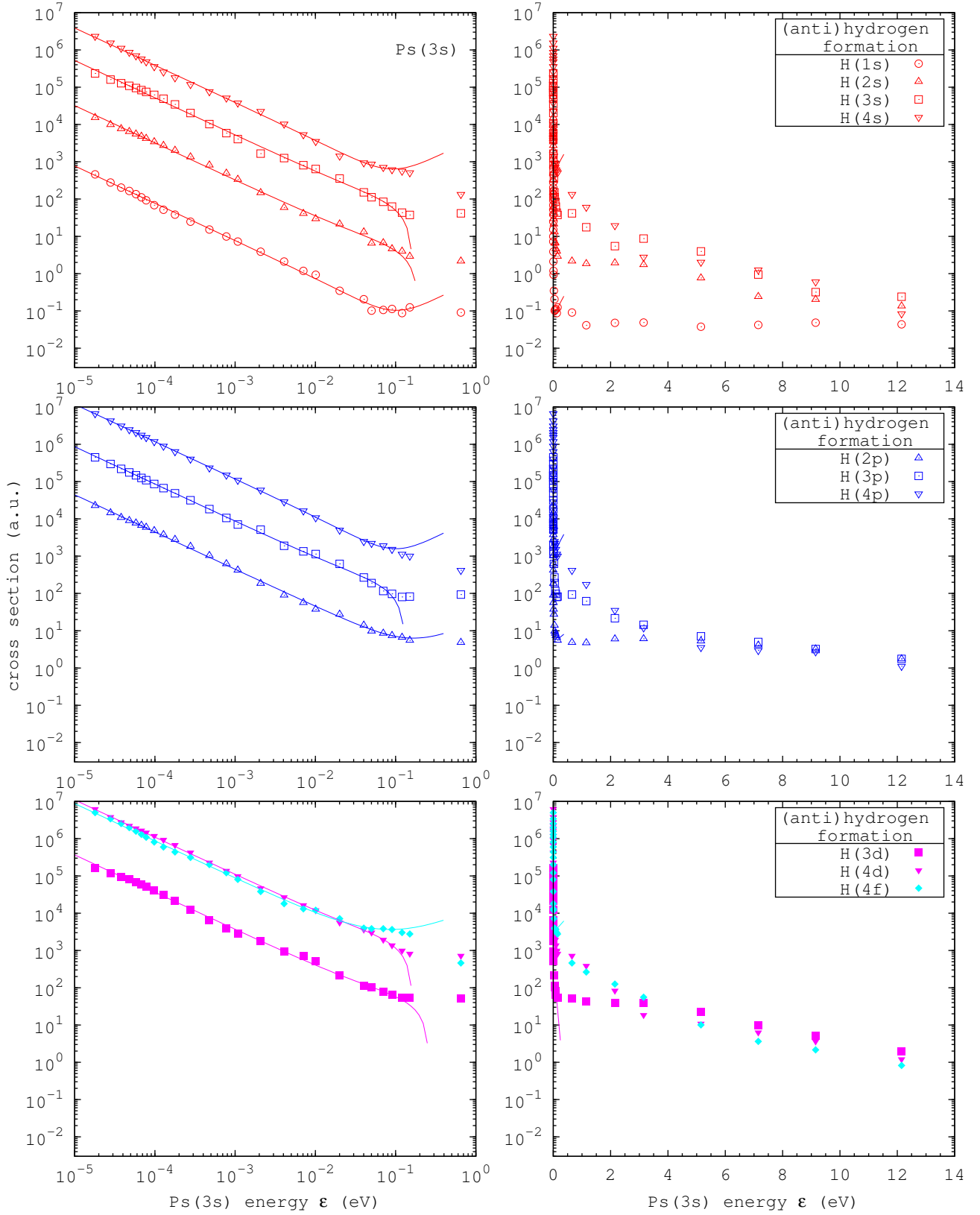


FIG. 5: (Color online) The cross sections for positronium in the 3s state scattering on (anti)protons to form (anti)hydrogen. The left side data are for scattering near zero energies for formation of hydrogen in s (top), p (middle) d or f states (bottom). The right side data are across a larger energy range. The solid lines for the near zero energy results are the least squares fits to the data up to 0.1eV with the fitted parameters given in table IV.

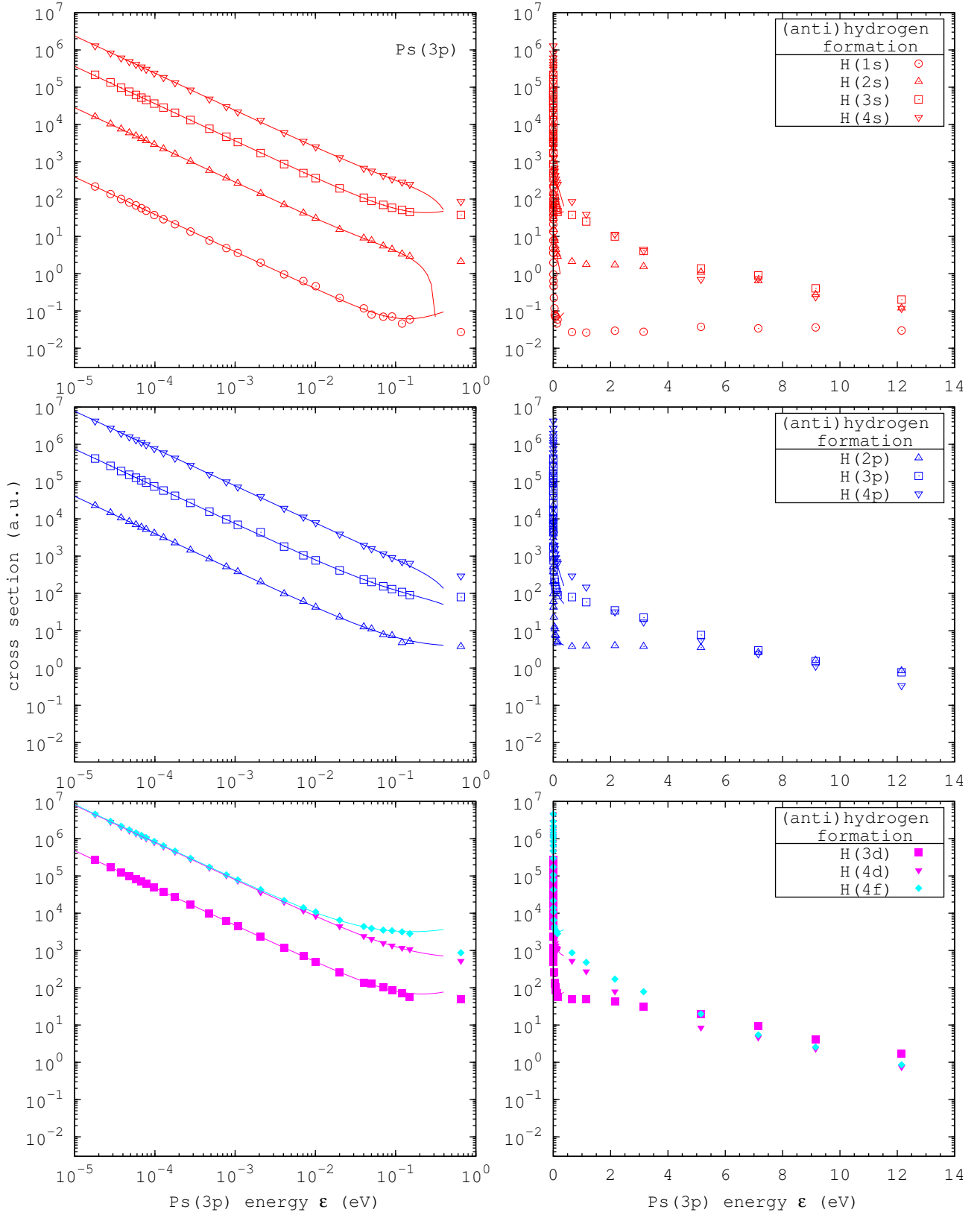


FIG. 6: (Color online) The cross sections for positronium in the $3p$ state scattering on (anti)protons to form (anti)hydrogen. The left side data are for scattering near zero energies for formation of hydrogen in s (top), p (middle) d or f states (bottom). The right side data cover a larger energy range. The solid lines for the near zero energy results are the least squares fits to the data up to 0.1eV with the fitted parameters given in table V.

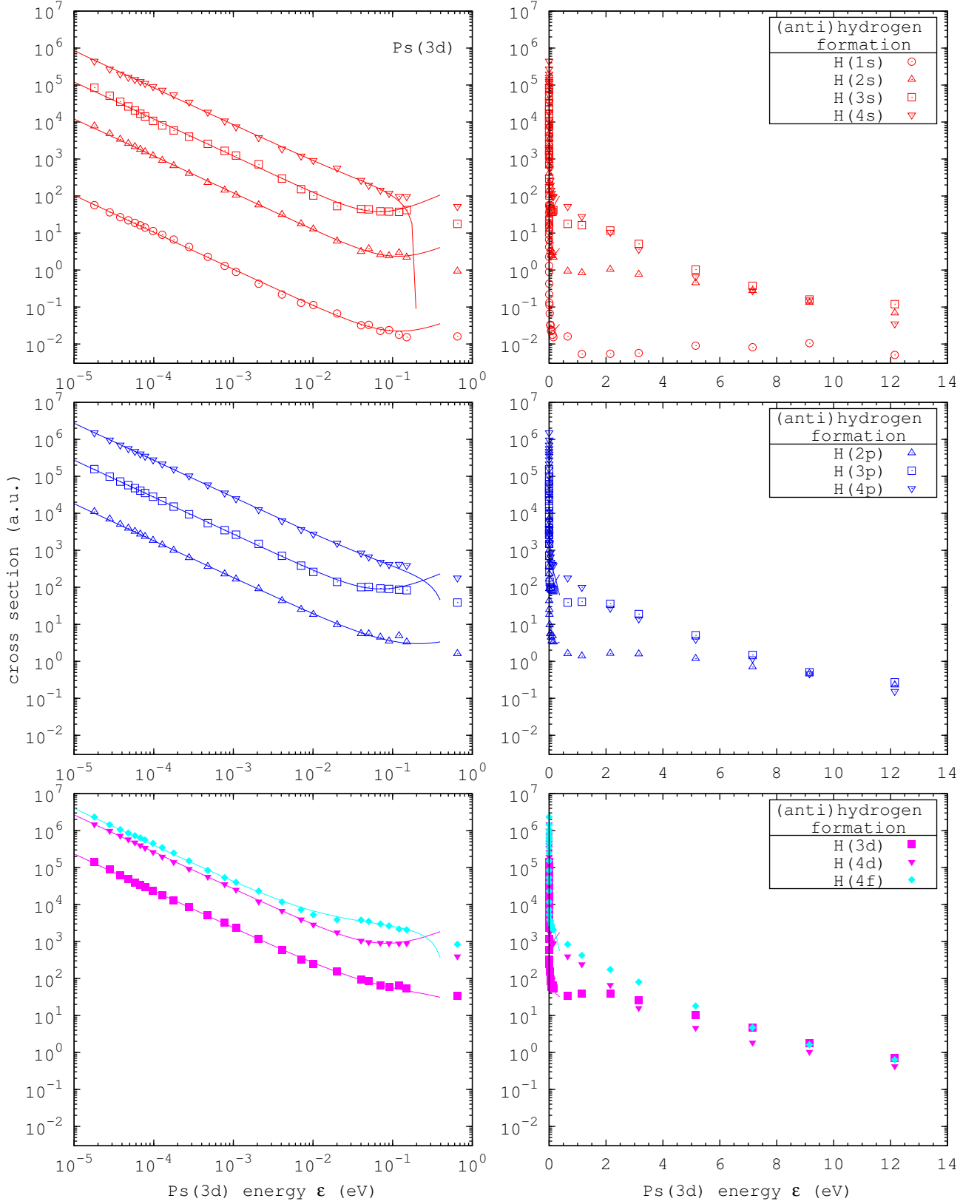


FIG. 7: (Color online) The cross sections for positronium in the 3d state scattering on (anti)protons to form (anti)hydrogen. The left side data are for scattering near zero energies for formation of hydrogen in *s* (top), *p* (middle) *d* or *f* states (bottom). The right side data are across a larger energy range. The solid lines for the near zero energy results are least squares fits of the data up to 0.1eV with the fitted parameters given in table VI.

aid in mitigating, for instance, motionally-induced complexities.

Currently, at least two groups (see e.g., [49, 50]) envisage using \bar{H} beams for studies of its gravitational properties, and for hyperfine spectroscopy, respectively. In particular, ASACUSA requires directed fluxes of low energy ground state \bar{H} for their intended measurements of the hyperfine splitting interval. Recent work by this group ([51]) has shown that a modest yield (80 \bar{H} atoms in total, at a rate of about 25 per hour and determined to be in a quantum state below $n = 29$) can be detected 2.7 m downstream of their cusp trap arrangement [52] for e^+ - \bar{p} mixing cycles of 15 minutes duration, each involving around 3×10^5 \bar{p} and 3×10^7 e^+ . In this experiment the \bar{H} was produced at low (antiparticle cloud) temperatures to exploit the three-body reaction $e^+ + e^+ + \bar{p} \rightarrow \bar{H} + e^+$ and the cusp trap magnetic field configuration resulted in beam-like emission from the production region by allowing low-field seeking \bar{H} to escape (and to some extent focussing it) along the axis of the system.

As mentioned earlier, an alternative method to produce an \bar{H} beam is to exploit reaction 1 by passing an antiproton beam through a Ps target. This reaction will, due to momentum considerations, be peaked in the original direction of the heavy projectile such that the angular properties of the \bar{H} beam will be governed by those of the incoming \bar{p} . In this respect, the cross section data presented in figures 2-7 span the Ps kinetic energy range from 10^{-5} eV to just over 10 eV, corresponding to an equivalent \bar{p} kinetic energy from around 10 meV to about 13 keV. The latter spans the range over which it should be feasible to produce controlled, virtually mono-energetic, \bar{p} beams extracted from trapped clouds and plasmas. This field has been pioneered by the ASACUSA collaboration that has developed techniques to manipulate \bar{p} , currently down as far as the 100-200 eV range [53–55], with applications in the keV region in atomic/molecular collision physics [56, 57]. In what follows we will consider cross sections at a single fixed Ps kinetic energy of 100 meV, which corresponds to an effective \bar{p} kinetic energy of just under 100 eV, with a speed of just over 10^5 ms^{-1} , for an idealised stationary Ps target. Thus we envision a collision geometry in which a near-mono-energetic \bar{p} beam crosses a Ps target in a confined gas-cell arrangement (see e.g. [8] for further details). Our work can be used to produce estimates of the intensity of \bar{H} beams derived from reaction 1. The examples we give are illustrative, and meant to offer guidance to experiment, rather than an attempt to predict the outcomes of what are likely to be complex experimental systems.

The first point to note from figure 2 is that for the Ps $1s$ state, formation into $\bar{H}(1s)$ is the only open channel at 100 meV, where it has a collision cross section of around 6 a.u.. The cross sections for Ps($2p$), Ps($3p$) and Ps($3d$) are given in figures 4, 6 and 7, from which three trends are apparent: (i) the cross sections for direct formation into the $\bar{H}(1s)$ state become depressed for the excited Ps targets; (ii) the production cross sections for excited \bar{H}

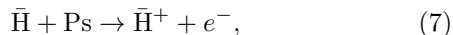
states increase dramatically with increasing Ps principal quantum number, and (iii) so does the number of different final \bar{H} states. Thus, it is apparent, in a gas cell arrangement in which \bar{p} collide with excited Ps atoms, that the yield of $\bar{H}(1s)$ will be dominated by the rapid population enhancement due to radiative decay of the excited \bar{H} states. For instance at the \bar{H} kinetic energy of 100 eV, a flight path of around 1 m is sufficient to ensure that almost all of the \bar{H} produced will be in the ground state. Indeed the only unavoidable losses are due to direct production of \bar{H} in the metastable $2s$ state, and decays to this level directly from the $4p$ and $3p$ states, and indirectly via $4s$ - $3p$ - $2s$ and $4d$ - $3p$ - $2s$ cascades. From the known lifetimes of the relevant transitions [58], it is straightforward to compute branching ratios for these, such that around 12% of each of the $4p$ and $3p$ populations are lost, together with 5% of the $4s$ and 3% of the $4d$. For instance, for the cross sections for the $3p$ Ps state shown in figure 6, this amounts to about a 4% loss from an overall production cross section of around 6000 a.u..

The production of excited state positronium atoms with principal quantum numbers in the range $n = 2$ -20 has been achieved recently in several laboratories [42, 43, 45, 59, 60]. Whilst absolute production efficiencies are difficult to extract, the measurements are consistent with yields in the region of 20% of the ground state population, and higher conversion rates (above around 30%) have been postulated [61]. Assuming the latter, it might then be feasible to create, using a gas cell geometry of the type envisaged by GBAR ([6–8]), an excited state ($3p$) Ps cloud with an effective density of around 10^{17} m^{-3} over a length of 1 cm. In this scenario, around 1.5% of the \bar{p} flux crossing such a target (obviously in a pulse to coincide with the Ps and its finite lifetime against annihilation and radiative decay) can be converted into a beam of $1s$ \bar{H} which, to first order, will retain the properties of the incident antiprotons. Incidentally, a $2s$ \bar{H} flux of around 0.07% of the incident \bar{p} s will be present in this beam. It is worth noting that it may be possible to obtain even higher yields using higher Ps principal quantum numbers, though there may be a trade-off with the length of the flight path required to ensure that the anti-atoms have reached the ground state.

The ASACUSA collaboration [50] is hoping to perform hyperfine spectroscopy on the $1s$ state of \bar{H} (which has a splitting of approximately 1420 MHz [62]) to obtain a linewidth of around 10 kHz, limited by the transit time of a 50 K beam (equivalent to around 5 meV) across a 10 cm long cavity. In fact this transit time broadening linewidth limit is given (in kHz) by $\Delta f_t \approx 14\sqrt{V}/d$ for a beam of kinetic energy (eV) and a cavity length, d . In the case discussed above, and assuming the 10 cm ASACUSA cavity length, we find $\Delta f_t \approx 1.4$ MHz. This is similar to the precision already achieved by ALPHA [62], however, the intensity of the \bar{H} beam would likely be much higher than can be achieved from the cusp trap arrangement (see above), with the prospect of finer line splitting leading to a more precise determination. Furthermore, if the \bar{p} (and

thus the \bar{H} beam kinetic energy could be reduced, there would be a double gain of a reduction in the broadening of the transition coupled with an enhancement in the \bar{H} flux, which should result in better line splitting.

The possibility, currently pursued by the GBAR collaboration ([6–8]), to study the gravitational interaction of antihydrogen by exploiting the free-fall of ultra-cold anti-atoms was already briefly mentioned in section I. In their scheme it is envisaged that the \bar{H} will be produced via a charge exchange scheme involving reaction (1) followed by the creation of the positive antihydrogen ion via,



with the \bar{H}^+ then captured and cooled before the positron is photoionized [16]. Due to the energetics of reaction (7) and the fact that \bar{H}^+ is expected to have only one state (as does its matter counterpart H^+) that is bound by around 0.75 eV with respect to $e^+ + \bar{H}$, reaction (7) is only probable when the colliding \bar{H} is in the ground state. The cross sections we have presented here can be used to derive estimates for the \bar{H}^+ yield (also given cross sections for reaction (7)), and in principle a full analysis of various scenarios can be undertaken in the manner described by Comini and co-workers [63], though this is beyond the scope of the present work. What we do point out is that if the enhanced rates of ground state \bar{H} are to be exploited by lowering the \bar{p} kinetic energy (from that currently envisaged in the few keV range), then due to threshold effects in heavy particle collisions (see e.g. [64]), the \bar{H} should collide with Ps in the $n = 3$ state, a variant of reaction (7) which is borderline exothermic. Thus, there is an urgent need for accurate cross sections for reaction (7) for excited Ps states, especially in the lower energy range covered by the present work.

B. Trapped Antihydrogen

In other experiments (for example ALPHA and ATRAP), a major goal is to hold \bar{H} in a magnetic minimum neutral atom trap to promote the detailed study of its properties. To date anti-atoms have been held, typically singly or in very low numbers [65, 66], in traps around 0.5 K deep and in some instances for time periods in excess of 1,000 s [67], which is more than enough time to ensure that any \bar{H} formed in an excited state from the aforementioned three-body reaction decays to the ground state. Major challenges to increase the yield of trapped \bar{H} are to cool the positrons and antiprotons to temperatures as low as possible (preferably to a level comparable to the neutral trap depth) before they are mixed to form the anti-atoms and to ensure that the low antiparticle temperatures are maintained during mixing (i.e., that the electrical manipulations required to overlap the species do not result in heating). Use of reaction (1)

may reduce the level of difficulty, as only cold antiprotons are required. In this respect the issue then becomes whether the resulting antihydrogen kinetic energy is low enough to allow trapping.

Experimentally, the \bar{H} must be formed, as at present, in a Penning-type charged particle trap which has a magnetic minimum neutral atom trap superimposed. Currently the Penning trap electrodes are cylindrical in nature and with a typical radius of 1-2 cm. To exploit reaction (1) the Ps should be formed at a surface as close as possible to the trapped antiproton cloud, with attendant laser access to provide for photo-excitation of the Ps prior to interaction. This is by no means a trivial problem, as specialised structures (e.g., porous silica [68]) are often used to create low energy (typically sub-100 meV) Ps and these must be integrated into the Penning trap structure.

In what follows, we have assumed that this can be achieved with modest losses of Ps flux such that useful yields of \bar{H} can be obtained. It is noteworthy that, for trapping, only the total \bar{H} formation cross section (i.e., not state-specific) is needed, as the trapped \bar{H} lifetime is sufficient to ensure that the ground state will be reached, if the anti-atom is held. In our previous work [21] we made estimates of \bar{H} yields for the Ps(3p) case, finding a few tens of antihydrogen atoms could be produced for a Ps density of 10^{15} m^{-3} and for Ps kinetic energies (with the \bar{p} assumed stationary) in the 10-100 meV range. It is clear from that work, and the data presented herein, that going to higher Ps principal quantum numbers will dramatically increase the \bar{H} production cross section, and hence the overall anti-atom yield. Indeed, if the factor of approximately 40 increase in cross section when going from the 2p to the 3p state is maintained to $n = 10$ Ps and above, then essentially all \bar{p} will interact to produce \bar{H} .

However, of paramount importance is not just the yield of \bar{H} , but also its kinetic energy, since this must be below the neutral trap depth if it is to be held. In this respect we have made some estimates of the \bar{H} recoil as a result of the \bar{p} -Ps reaction. We assume that the \bar{p} is stationary, and in one (ideal) limit that so too is the Ps. In this case the recoil of the \bar{H} is a result of the energy difference between the relevant Ps and \bar{H} energy levels, which we denote as $Q = \epsilon_{nl}^{\bar{H}} - \epsilon_{nl}^{\text{Ps}}$. It is easy to show that, in this limit the effective \bar{H} recoil temperature, $T_{\bar{H}}$, is given by [15]

$$T_{\bar{H}} = \frac{2Qm_e}{3m_{\bar{H}}k_B} = \frac{2m_eR}{3m_{\bar{H}}k_B} \left(\frac{1}{n_{\bar{H}}^2} - \frac{1}{2n_{\text{Ps}}^2} \right). \quad (8)$$

Here m_e and $m_{\bar{H}}$ are the electron/positron and \bar{H} masses respectively, k_B is Boltzmann's constant and R the Rydberg, with $n_{\bar{H}}$ and n_{Ps} now explicitly distinguished by notation as the \bar{H} and Ps principal quantum numbers. For the antihydrogen to be held in a trap of effective wall temperature, T_W , clearly $T_{\bar{H}} \leq T_W$. From this requirement, and substituting values for the constants, it

can be shown that the antihydrogen state constraint is given by

$$n_{\bar{H}} \geq \sqrt{2}n_{Ps} \left(1 + \frac{n_{Ps}^2 T_W}{28.7}\right)^{-1/2}, \quad (9)$$

with T_W in degrees K. The ALPHA neutral atom trap is around 0.5 K deep [65], and inserting this value into equation 9 it is easy to show that for $n_{Ps} = 3$, antihydrogen states with $n_{\bar{H}} \geq 4$ will be trapped. If more highly excited states of Ps can be produced then a larger selection of energy-allowed \bar{H} states can be trapped: as an example, all states with $n_{\bar{H}} \geq 9$ will be trapped for $n_{Ps} = 10$. Bearing in mind that the \bar{H} states most likely to be populated are those that are as close to energy-degenerate with the starting Ps states as possible (formally satisfied when $n_{\bar{H}} = \sqrt{2}n_{Ps}$), then it is clear that, as n_{Ps} is increased, a progressively larger fraction of the \bar{H} produced has a low enough kinetic energy to allow trapping, when only the magnitude of Q is considered.

Another limit is to presume that the Ps possesses a kinetic energy, K_{Ps} , but that $Q = 0$; i.e., for the latter that the \bar{H} and Ps binding energy difference can be ignored, which will become an approachable limit as n_{Ps} is increased. Here the classical equations for the conservation of momentum and energy yield somewhat cumbersome expressions that depend upon the angle between the initial Ps velocity and that of the \bar{H} in the final state (or that of the ejected electron). However, it is straightforward to show that the maximum \bar{H} recoil kinetic energy, $K_{\bar{H}}$, is of the order of $10 \times m_e K_{Ps}/m_{\bar{H}}$ [15]. Equating $K_{\bar{H}} = 3k_B T_W/2$, the effective value of K_{Ps} which results in \bar{H} with a kinetic energy low enough to be trapped is given, approximately, by $K_{Ps} = 3k_B T_W m_{\bar{H}}/20em_e$, with e the elementary charge. Again taking $T_W = 0.5$ K and inserting values for the constants, we find $K_{Ps} \approx 12$ meV, or an approximate temperature equivalent of 180 K. Though this requires positronium at energies lower than room temperature, Ps sources that operate in the cryogenic environments typical of Penning traps have

been developed [69–71], however it is likely that further work is required, perhaps involving laser cooling [72], to ensure that the Ps interacts at correspondingly low kinetic energies. When both $T_{Ps} \neq 0$ and $Q \neq 0$ the situation is more involved, though the kinematics of the collision outcome can be simulated [73], if the relevant differential cross sections are known.

V. CONCLUSIONS

We have performed calculations of positronium scattering on (anti)protons to produce (anti)hydrogen for various initial $n \leq 3$ states to final $n \leq 4$ states. The largest cross sections are obtained for the $3 \rightarrow 4$ transitions, with minor variation across the different l . Threshold laws have been found to be strictly valid at threshold, with simple formulae given to yield accurate ($\pm 5\%$) results from zero to about 0.1 eV incident Ps energy, which is of practical value to experiments attempting to form antihydrogen, both in beams and held in traps. We have discussed aspects of the impact of the present work on those endeavours.

Presently, we are developing novel approaches to the solution of the two-center CCC equations that will reduce the ill-conditioning, and also implementing numerical approaches that will manage even more ill-conditioned systems. If successful, we hope to extend the calculations to states with higher principal quantum numbers.

Acknowledgments

The Curtin authors are grateful for the support of the Australian Research Council, the National Computing Infrastructure and The Pawsey Supercomputer Center. A.S.K. acknowledges partial support from the U.S. National Science Foundation under Award No. PHY-1415656. M.C. is indebted to the EPSRC (UK) for the support of his antimatter work.

-
- [1] K. A. Olive *et al.* (Particle Data Group), Chinese Phys. C **38**, 1 (2014).
 - [2] W. A. Bertse, E. Butler, M. Charlton, and N. Madsen, J. Phys. B: At. Mol. Opt. Phys. **48**, 232001 (2015).
 - [3] M. Charlton, J. Eades, D. Horváth, R. Hughes, and C. Zimmermann, Physics Reports **241**, 65 (1994).
 - [4] M. H. Holzschleiter, M. Charlton, and M. M. Nieto, Phys. Rep. **402**, 1 (2004).
 - [5] M. Hori and J. Walz, Prog. Part. Nucl. Phys. **72**, 206 (2013).
 - [6] GBAR collaboration, Proposal to measure the gravitational behaviour of antihydrogen at rest: GBAR **CERN SPSC-P-342** (2011).
 - [7] P. Pérez and Y. Sacquin, Class. Quant. Grav. **29**, 184008 (2012).
 - [8] D. P. van der Werf, Int. J. Mod. Phys.: Conference Series **30**, 1460263 (2014).
 - [9] Nuclear Instruments and Methods in Physics Research Section B: Beam Interactions with Materials and Atoms **266**, 351 (2008).
 - [10] M. Doser *et al.*, Class. Quant. Grav. **29**, 184009 (2012).
 - [11] C. Amole *et al.*, Nature Communications **4**, 1785 (2013).
 - [12] J. W. Humberston, M. Charlton, F. M. Jacobsen, and B. I. Deutch, J. Phys. B: At. Mol. Phys. **20**, L25 (1987).
 - [13] M. Charlton, Phys. Lett. A **143**, 143 (1990).
 - [14] D. Krasnický *et al.*, Int. J. Mod. Phys.: Conference Series **30**, 1460262 (2014).
 - [15] B. I. Deutch, M. Charlton, M. H. Holzschleiter, P. Hvelplund, L. V. Jørgensen, H. Knudsen, G. Laricchia, J. P. Merrison, and M. R. Poulsen,

- Hyperfine Interactions **76**, 151 (1993).
- [16] J. Walz and T. W. Hänsch, *Gen. Rel. Grav.* **36**, 561 (2004).
- [17] The GBAR collaboration, Report No. SPSC-P-342 (2011).
- [18] E. P. Wigner, *Phys. Rev.* **73**, 1002 (1948).
- [19] I. I. Fabrikant, *J. Phys. B* **7**, L259 (1974).
- [20] H. R. Sadeghpour, J. L. Bohn, M. J. Cavagnero, B. D. Esry, I. I. Fabrikant, J. H. Macek, and A. R. P. Rau, *J. Phys. B* **33**, R93 (2000).
- [21] A. S. Kadyrov, C. M. Rawlins, A. T. Stelbovics, I. Bray, and M. Charlton, *Phys. Rev. Lett.* **114**, 183201 (2015).
- [22] J. P. Merrison, H. Bluhme, J. Chevallier, B. I. Deutch, P. Hvelplund, L. V. Jorgensen, H. Knudsen, M. R. Poulsen, and M. Charlton, *Phys. Rev. Lett.* **78**, 2728 (1997).
- [23] J. W. Humberston, P. V. Reeth, M. S. T. Watts, and W. E. Meyerhof, *J. Phys. B* **30**, 2477 (1997).
- [24] J. Mitroy, *Aust. J. Phys.* **46**, 751 (1993).
- [25] J. Mitroy and A. T. Stelbovics, *J. Phys. B* **27**, L55 (1994).
- [26] J. Mitroy, *Aust. J. Phys.* **48**, 645 (1995).
- [27] J. Mitroy, *Aust. J. Phys.* **48**, 893 (1995).
- [28] J. Mitroy, *Phys. Rev. A* **52**, 2859 (1995).
- [29] N. Yamanaka and Y. Kino, *Nuclear Instruments and Methods in Physics Research Section B: Beam Interactions with Materials and Atoms* **214**, 40 (2004).
- [30] P. Comini and P.-A. Hervieux, *New J. Phys.* **15**, 095022 (2013).
- [31] A. S. Kadyrov and I. Bray, *Phys. Rev. A* **66**, 012710 (2002).
- [32] J. J. Bailey, A. S. Kadyrov, and I. Bray, *Phys. Rev. A* **91**, 012712 (2015).
- [33] I. Bray and A. T. Stelbovics, *Phys. Rev. A* **48**, 4787 (1993).
- [34] I. Bray and A. T. Stelbovics, *Phys. Rev. A* **49**, R2224 (1994).
- [35] H. Wu, I. Bray, D. V. Fursa, and A. T. Stelbovics, *J. Phys. B* **37**, L1 (2004).
- [36] D. V. Fursa and I. Bray, *New J. Phys.* **14**, 035002 (2012).
- [37] M. C. Zammit, D. V. Fursa, and I. Bray, *Phys. Rev. A* **87**, 020701 (2013).
- [38] A. S. Kadyrov, A. V. Lugovskoy, R. Utamuratov, and I. Bray, *Phys. Rev. A* **87**, 060701 (2013).
- [39] A. Bray, I. Abdurakhmanov, A. Kadyrov, D. Fursa, and I. Bray, *Comp. Phys. Comm.* **196**, 276 (2015).
- [40] “Arbitrary precision computation package,” <http://crd-legacy.lbl.gov/~dhbailey/mpdist/>.
- [41] I. B. Abdurakhmanov, A. S. Kadyrov, and I. Bray, *Phys. Rev. A*, submitted (2015).
- [42] D. B. Cassidy, T. H. Hisakado, H. W. K. Tom, and A. P. Mills Jr, *Phys. Rev. Lett.* **108**, 043401 (2012).
- [43] A. C. L. Jones, T. H. Hisakado, H. J. Goldman, H. W. K. Tom, A. P. Mills Jr, and D. B. Cassidy, *Phys. Rev. A* **90**, 012503 (2014).
- [44] S. Cialdi, I. Boscolo, F. Castelli, F. Villa, G. Ferrari, and M. G. Giammarchi, *Nuc. Instrum. Meth. B* **269**, 1527 (2011).
- [45] S. Aghion *et al.* (AEgIS Collaboration), *Phys. Rev. Lett.* **submitted** (2015).
- [46] N. F. Ramsey, *Molecular Beams* (Oxford, Clarendon Press, 1956).
- [47] N. F. Ramsey, *Rev. Mod. Phys.* **62**, 541 (1990).
- [48] C. J. Foot, *Atomic Physics* (Oxford Master Series in Atomic, Optical and Laser Physics, Oxford University Press, 2005).
- [49] M. Doser *et al.* (AEgIS Collaboration), *J. Phys. Conf. Ser.* **199**, 012009 (2010).
- [50] E. Widmann *et al.*, *Hyperfine Interact.* **215**, 1 (2013).
- [51] N. Kuroda *et al.*, *Nature Commun.* **5**, 3089 (2014).
- [52] Y. Enomoto *et al.*, *Phys. Rev. Lett.* **105**, 243401 (2010).
- [53] N. Kuroda *et al.*, *Phys. Rev. Lett.* **94**, 023401 (2005).
- [54] N. Kuroda *et al.*, *Phys. Rev. Lett.* **100**, 203402 (2008).
- [55] N. Kuroda *et al.*, *Phys. Rev. Special Topics-Accelerators and Beams* **15**, 024702 (2012).
- [56] H. Knudsen, H.-P. E. Kristiansen, H. D. Thomsen, U. I. Uggerhøj, T. Ichioka, S. P. Møller, C. A. Hunniford, R. W. McCullough, M. Charlton, N. Kuroda, Y. Nagata, H. A. Torii, Y. Yamazaki, H. Imao, H. H. Andersen, and K. Tökesi, *Phys. Rev. Lett.* **101**, 043201 (2008).
- [57] H. Knudsen *et al.*, *Phys. Rev. Lett.* **105**, 213201 (2010).
- [58] H. A. Bethe and E. E. Salpeter, *Quantum Mechanics of One- and Two-Electron Systems* (Springer-Verlag, Berlin, 1957).
- [59] T. E. Wall, A. M. Alonso, B. S. Cooper, A. Deller, S. D. Hogan, and D. B. Cassidy, *Phys. Rev. Lett.* **114**, 173001 (2015).
- [60] C. J. Baker, D. Edwards, C. A. Isaac, and D. P. van der Werf, private communication (2015).
- [61] F. Castelli, I. Boscolo, S. Cialdi, M. G. Giammarchi, and D. Comparat, *Phys. Rev. A* **78**, 052512 (2008).
- [62] C. Amole *et al.* (ALPHA Collaboration), *Nature* **483**, 439 (2012).
- [63] P. Comini, P.-A. Hervieux, and F. Biraben, *Hyperfine Interact.* **228**, 159 (2014).
- [64] H. S. W. Massey and H. B. Gilbody, *Electronic and Ionic Impact Phenomena Volume IV* (Oxford, Clarendon Press, 1974).
- [65] G. B. Andresen *et al.* (ALPHA Collaboration), *Nature* **468**, 673 (2010).
- [66] G. Gabrielse *et al.* (ATRAP Collaboration), *Phys. Rev. Lett.* **108**, 113002 (2012).
- [67] G. B. Andresen *et al.* (ALPHA Collaboration), *Nature Phys.* **7**, 558 (2011).
- [68] L. Liskay *et al.*, *Appl. Phys. Lett.* **92**, 063114 (2008).
- [69] D. B. Cassidy, P. Crivelli, T. H. Hisakado, V. E. Liskay, L. Melling, P. Perez, H. W. K. Tom, and A. P. Mills Jr, *Phys. Rev. A* **81**, 012715 (2010).
- [70] D. B. Cassidy, T. H. Hisakado, H. W. K. Tom, and A. P. Mills Jr, *Phys. Rev. Lett.* **107**, 033401 (2011).
- [71] S. Mariazzi, A. Salemi, and R. S. Brusa, *Phys. Rev. A* **78**, 085428 (2008).
- [72] E. P. Liang and C. D. Dermer, *Opt. Comm.* **65**, 419 (1988).
- [73] D. B. Cassidy, J. P. Merrison, M. Charlton, J. Mitroy, and G. Ryzhikh, *J. Phys. B: At. Mol. Opt. Phys.* **32**, 1923 (1999).